



## Article

# Numerical Modeling and Nonlinear Finite Element Analysis of Conventional and 3D-Printed Spinal Braces

Iason Rossetos <sup>1</sup>, Charis J. Gantes <sup>1</sup> , George Kazakis <sup>2</sup>, Stefanos Voulgaris <sup>2</sup>, Dimitrios Galanis <sup>3</sup>, Fani Pliarchopoulou <sup>3</sup>, Konstantinos Soultanis <sup>3</sup> and Nikos D. Lagaros <sup>2,\*</sup> 

<sup>1</sup> Institute of Steel Structures, National Technical University of Athens, 157 73 Athens, Greece; iasonas.ross@gmail.com (I.R.); chgantes@central.ntua.gr (C.J.G.)

<sup>2</sup> Institute of Structural Analysis and Antiseismic Research, National Technical University of Athens, 157 73 Athens, Greece; kzkgeorge@gmail.com (G.K.); stefanosvoulg@gmail.com (S.V.)

<sup>3</sup> School of Medicine, National and Kapodistrian University of Athens, 115 27 Athens, Greece; dkgalanis@gmail.com (D.G.); fpl010@otenet.gr (F.P.); ksoultanis@otenet.gr (K.S.)

\* Correspondence: nlagaros@central.ntua.gr; Tel.: +30-6936118226

**Abstract:** This study aims to describe the numerical modeling and nonlinear finite element analysis of typical spinal braces as a first step towards optimizing their topology for 3D printing. Numerical simulation was carried out in Abaqus CAE software Version 2021, utilizing a CAD (Meshmixer Version 3.5.474) scan of an actual spinal brace. Boundary conditions were defined by means of contact surfaces between the human body and the supporting pads located in the interior of the brace. The process of tightening the straps on the rear face of the brace was simulated via appropriate imposed displacements. The response is described through the deformations and developing stresses of the brace and the contact pressures in the areas of interaction with the human body. Parametric analysis indicated that increasing the cross-sectional thickness or elastic modulus of the brace material results in higher maximum von Mises stresses and lower displacements. The comparison between 3D-printed and conventional braces highlighted the potential of 3D-printing technology to achieve comparable performance with customized designs, leveraging the constitutive properties of 3D-printed material obtained from tension tests. The tension tests demonstrated that the 3D-printed material achieved higher values of modulus of elasticity compared to traditional brace materials. Finally, the topology optimization criteria to be applied for the design of spinal braces in the next step of this ongoing research are briefly described.

**Keywords:** spinal brace; finite element analysis; nonlinear analysis; contact nonlinearity; laser scanning; topology optimization; 3D printing



**Citation:** Rossetos, I.; Gantes, C.J.; Kazakis, G.; Voulgaris, S.; Galanis, D.; Pliarchopoulou, F.; Soultanis, K.; Lagaros, N.D. Numerical Modeling and Nonlinear Finite Element Analysis of Conventional and 3D-Printed Spinal Braces. *Appl. Sci.* **2024**, *14*, 1735. <https://doi.org/10.3390/app14051735>

Academic Editors: Zhonghua Sun and Claudio Belvedere

Received: 29 December 2023

Revised: 13 February 2024

Accepted: 17 February 2024

Published: 21 February 2024



**Copyright:** © 2024 by the authors. Licensee MDPI, Basel, Switzerland. This article is an open access article distributed under the terms and conditions of the Creative Commons Attribution (CC BY) license (<https://creativecommons.org/licenses/by/4.0/>).

## 1. Introduction

Ancient skeletal remains of “upright” humans reveal evidence of spinal diseases and deformities predating antiquity. It was Hippocrates (460–375 BC) who used the terms “scoliosis” and “kyphosis”, along with “lordosis”, to describe the deformities of the spine in his work *On the Joints* [1]. The basic engineering principles of early spinal braces still apply to modern ones, such as three-point bending and inversion forces [2].

As of now, the most commonly used scoliosis braces are the Boston Brace and the Milwaukee Brace [3–5]. Both braces are manufactured using a combination of thermoplastics (polyethylene or polypropylene), foam liners, and straps. To manufacture the brace, the thermoplastic is heated to mold the plastic sheet into the shape of the patient’s body, foam liners are placed in contact areas where the main pressure is applied, and then straps are used to adjust and secure the brace. The manufacturing process, especially the molding of the thermoplastic, is quite complicated and leaves much to be desired in terms of precision.

Efforts are currently in progress to advance the design of modern spinal braces with a primary focus on ensuring patient comfort and usability. To achieve this goal, the inte-

gration of laser scanning is necessary for the design of personalized spinal braces. Laser scanning technology provides a noninvasive and precise means of capturing detailed anatomical information, making it valuable for custom product design in medical applications [6,7]. This detailed digital representation serves as the dataset for the subsequent design phases. The ability to consider all torso nuances enables the creation of braces that are tailor made to accommodate the patient's anatomy. This personalized approach, facilitated by laser scanning, should not only enhance the efficacy of spinal braces but also contribute to heightened patient comfort and adherence.

In recent years, 3D-printing technology has started to be experimented with in the orthopedic field. Some notable applications include the manufacturing of spinal braces, bone splints, and customized prosthetics [8–16]. Several researchers have proposed procedures integrating advanced design methods and additive manufacturing for the realization of lightweight, easy-to-use personalized braces. Among them, Ronca et al. [10] presented a comparative study using four different materials in the 3D-printing process and evaluated their performance to conclude which one is more suitable for a 3D-printed spinal brace. Redaelli et al. [14] performed a study for the evaluation of the advantages and disadvantages of 3D-printed spinal braces in comparison to the traditional ones using different evaluation criteria. Among the many different parameters of the 3D-printing techniques a particularly important aspect refers to material selection. This much-needed parameter of the mechanical properties of 3D-printed polymers has been studied in [12–15], also addressing the very significant issues of reliability and fatigue. Furthermore, Mafi et al. [16] compared the performance of three varied materials simulating a spinal brace in the finite element analysis software Abaqus.

A necessary step towards optimizing the brace in terms of weight and comfort is the numerical modeling and simulation of its interaction with the patient's body using the finite element method, enabling the estimate of the developing deformations and stresses of the brace as well as the developing pressures on the body during the brace's use. For that purpose, the geometry, material properties, and interaction properties must be modeled.

When addressing the simulation of boundary conditions, various simplified approaches employing pinned or fixed supports have been explored in previous works [16,17]. However, this approach overestimates the local stresses in the vicinity of such supports. In the present study, we aim for a more intricate simulation of the interaction between the spinal brace and the body, introducing a level of complexity that renders the problem nonlinear. The exploration of nonlinearity, particularly arising from contact, aligns with the investigations found in other publications [18–20], where efforts have been made to simulate the contact between the trunk and the skeleton. This nuanced approach adds depth to our study, contributing to a more comprehensive understanding of the complexities involved in spinal brace simulations.

The objective of the present study is to investigate the application of numerical modeling and nonlinear finite element analysis as a first step towards the subsequent topology optimization-based design of spinal braces to be manufactured using 3D-printing technology. The methodology encompasses the creation of a numerical simulation using Abaqus CAE software [21], leveraging a CAD scan derived from an existing spinal brace. To accurately represent real-world scenarios, realistic loads and boundary conditions are specified, with brace loads emulated through forced displacements, simulating the tension induced by tightening straps on the brace's rear surface. Furthermore, a parametric analysis is undertaken, exploring diverse values for the cross-sectional thickness and elastic modulus of the brace material, including the constitutive laws of 3D-printed material, properly determined by means of tension tests.

## 2. Numerical Modeling and Analysis

The brace and its interaction with the patient's body are simulated using the finite element method to calculate the developing deformations and stresses of the brace as well as the contact pressures between the brace and the body during the brace's use. For that

purpose, the geometry, material properties, and interaction properties must be modeled. A brief description of the fundamental concepts of numerical modeling and analysis is presented next to enable nonexpert readers to follow the proposed approach.

### 2.1. Laser Scanning Procedure

Laser scanning of the human torso involves the use of three-dimensional (3D) imaging technology to create a highly detailed digital representation of the upper body, including the chest and spine. The procedure follows these general steps: (i) Patient Preparation: During the scanning process, the patient must wear appropriate clothing, avoiding loose or reflective clothing, to ensure accurate data capture. (ii) Scanner Calibration: The laser scanning equipment is calibrated to ensure precision and accuracy according to instructions by the manufacturer. (iii) Patient Placement: The patient is placed in a designated area, and the laser scanning device is positioned to capture the upper body. (iv) Laser Scanning Process: The scanner emits laser beams onto the surface of the upper body. These lasers create a point cloud by measuring the distance between the scanner and the surface at various points. As the scanner moves or rotates, it captures data from different angles to build a comprehensive 3D model. Multiple scanning passes may be used to ensure complete coverage and accuracy. (v) Data Registration: The collected point cloud data is then aligned to ensure that all scans are properly combined to form a cohesive and accurate 3D representation. (vi) Mesh Generation: The point cloud data is converted into a mesh, a continuous surface composed of interconnected triangles. This mesh represents the detailed geometry of the scanned torso.

### 2.2. Conversion of Scanning File to Suitable Form

To model the spinal brace, the first step involves converting the scanning file into a suitable form. One of the primary challenges encountered during the formulation of scanned geometries is the presence of abrupt changes in certain parts of the domain. These changes can impede the modeling process of the spinal brace and therefore need to be addressed before proceeding with the modeling. Smoothing procedures are the key tool for eliminating these geometric irregularities. In the context of the spinal brace presented in this study, the primary focus was on addressing geometric abnormalities along the edges of the scanned spinal brace. Figure 1 illustrates schematic representations of both the original and smoothed domains using the CAD software Meshmixer by AutoDesk [22]. In addition to the smoothing procedure, the thickness of the original geometry is removed to enable the use of shell finite elements.

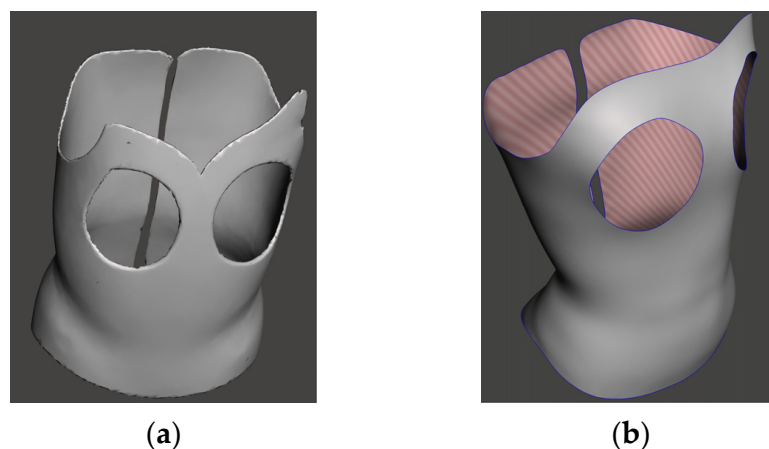


**Figure 1.** (a) Original scanned spine base. (b) Final smoothed model.

### 2.3. Modeling Details

The first step of the simulation process in the presented approach was to import into Abaqus finite element software the CAD file of a typical spinal brace obtained by laser scanning and subsequent conversion described in Section 2.2 for further processing. A numerical model of the spine with shell finite elements has been created, in which a cross-sectional thickness equal to 4 mm has been assigned (Figure 2a). Due to the complexity of the geometry of the brace, the abundance of curves, and general nonsymmetry, individual surfaces have been defined on the brace to achieve a better overview and higher accuracy for imposing loads and boundary conditions. For that purpose, the brace has been divided by planes parallel to the planes formed by the three main axes (Figure 2b).

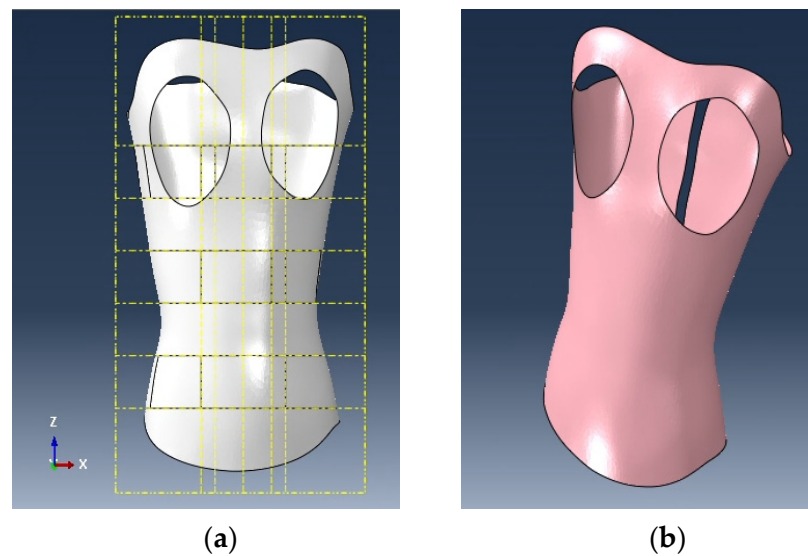


**Figure 2.** (a) CAD representation of spinal brace. (b) Division of the brace into individual surfaces to facilitate assignment of loads and boundary conditions.

**Material:** Conventional spinal braces are commonly manufactured using materials such as polypropylene, polyethylene, and their variants. In a study by Yun Hwan et al. [23], the elastic properties of polypropylene/ultra-high molecular weight polyethylene fiber were estimated, yielding a calculated value of approximately 1325 MPa. Additionally, the mechanical properties of materials used in traditional braces have been identified through experimental investigations in various studies [16,17,23,24]. One of the key objectives of this study is to conduct a comparative analysis between traditional brace materials and those produced through additive manufacturing, particularly utilizing 3D-printed PLA. Consequently, polypropylene is initially chosen as the material for the spinal brace in the traditional context, featuring a modulus of elasticity ( $E$ ) of 1000 MPa and a Poisson's ratio ( $\nu$ ) of 0.2.

**Support and Load Conditions:** This study builds upon the foundational work outlined in the work by Liao et al. [18], aiming to simulate the structural behavior of a spinal brace in order to further refine and develop the scenario presented. The primary focus lies in optimizing the brace's topology, aligning with a key loading scenario akin to the Boston brace. In particular, the simulation in this study replicates the application of corrective forces generated by pulling the straps on the back of the brace. This action effectively tightens the brace around the human body, inducing corrective forces within the patient's body that serve to limit the progression of spinal inclination. The mechanism involves the transmission of these corrective forces through supporting pads situated on the inner part of the brace, facilitating a more even distribution of contact pressures. This approach is instrumental in achieving a smoother and more targeted application of corrective forces, contributing to the overall effectiveness of the spinal brace in managing spinal alignment.



The developing tension of the tightening straps has been simulated in the model by imposing horizontal displacements in the tangential direction on the rear face of the brace, equal to 10 mm, as shown in Figures 3a and 4a. The clearance at the back of this specific brace is approximated to be in the range of 20–25 mm. The choice of imposed displacements of 10 mm on both sides of the rear face of the guardrail, as illustrated in Figure 3b, is based on the logical scenario of tensioning the straps until this clearance is filled.

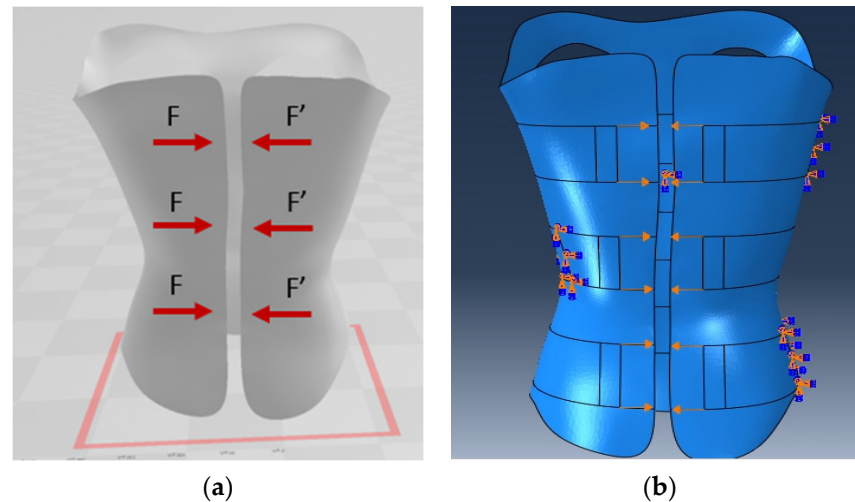


**Figure 3.** (a) Schematic illustration of the forces of the tethering straps on the rear face of the brace. (b) Imposed displacements and boundary conditions in the numerical simulation of the brace.

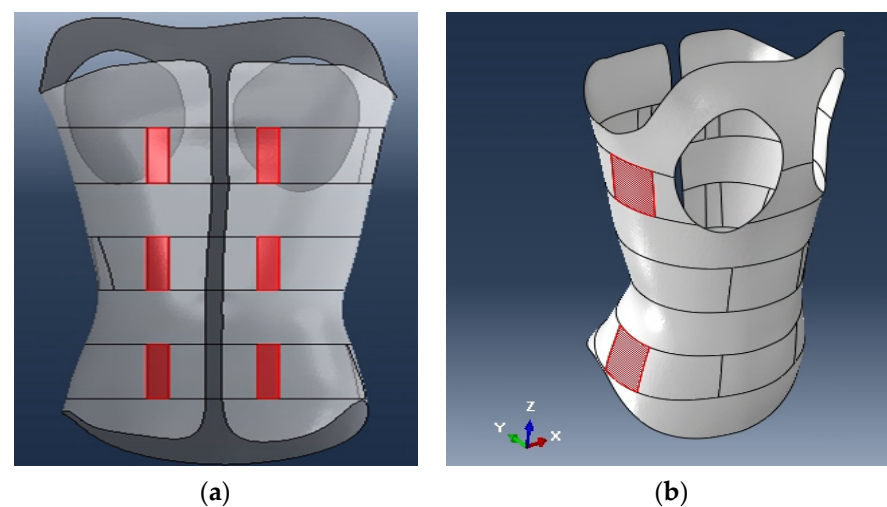


**Figure 4.** (a) Surfaces of attachment points of the straps at the rear face of the spinal brace. (b) Surfaces of supporting pads of the spinal brace.

A key element of the numerical modeling of the brace is the simulation of its interaction with the human body. During the patient's movement, the brace-pad system (Figures 4b and 5) presses the human body to develop corrective forces. Pressures, normal to the contact surface, develop in part of the interaction surfaces, while the remaining part of the pad surfaces moves away and loses contact with the human skin, and zero pressure develops. At the same time, friction between the body and the brace develops in tangential directions over the contact surfaces. This form of interaction is encountered in several engineering problems and is simulated by an interaction law, perpendicular to the contact direction, known as the pressure-overclosure relation (Figure 6). Information on the stiffness of human skin was obtained from Graham [25] and Cua [26]. To that effect, a new covariant surface of the surface of the brace is created to represent the human body. A new

part is created with exactly the same geometry as the brace, having mechanical properties  $E = 100\text{MPa}$ ,  $\nu = 0.45$  [14,18,19] in order to simulate the aforementioned interaction. The two parts interact through the defined surfaces of the supporting pads.

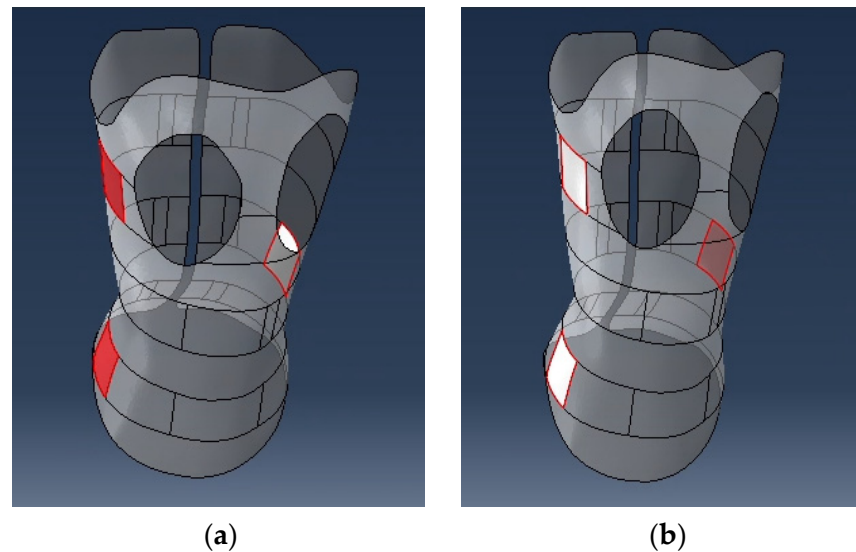


**Figure 5.** Description of the interaction surfaces between the brace and the human body. (a) Inner sides of the surfaces of supporting pads. (b) Outer sides of the surfaces of the human body.

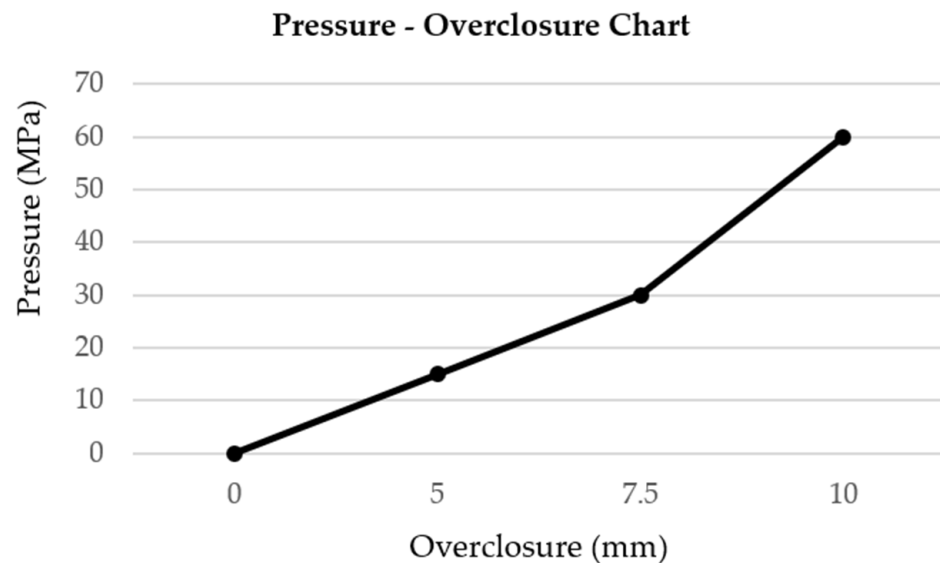


**Figure 6.** Pressure–overclosure chart describing the law of the brace–body interface in the pressure direction.

#### 2.4. Analysis Details

There are three potential sources of nonlinearity in structural engineering simulations, material, geometry, and boundary condition nonlinearity, corresponding, respectively, to cases where stresses exceed the linear part of the material law, large deformations develop so that the deformed geometry differs substantially from the undeformed one, and when boundary conditions change during the analysis. The loads and stresses that the brace is subjected to in its daily use by a patient do not usually produce significant stresses of the material [16,27–29], while the developing deformations are also limited by the patient’s body. For this reason, the prevailing type of nonlinearity is the one of the brace’s boundary conditions, namely its interaction with the patient’s body, which is described by the nonlinear pressure–overclosure chart of Figure 6.

To accommodate nonlinearity, full Newton's method is chosen as the numerical technique for solving the nonlinear equilibrium equations, as it offers better convergence rates compared to those exhibited by alternate methods for the types of nonlinear problems most often studied with ABAQUS. The maximum number of increments is taken as 100, the initial increment size is 0.1, and the minimum and maximum values of increment are 0.1, respectively.

### 2.5. Analysis Results

The analysis described above allows for the study of the displacements in the three axes over the entire surface of the brace, the developing stresses in the brace, which are critical for optimizing the required brace thickness, as well as the contact pressures (Figure 7) developing between the brace and the body, which are needed to evaluate the patient's comfort. The results are illustrated in the following figures:

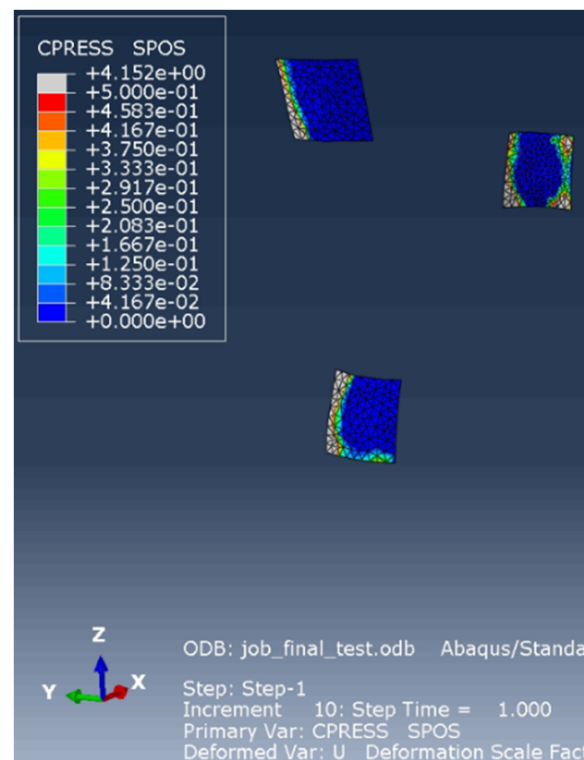


**Figure 7.** Contact pressures on the surfaces representing the human body (First numerical model).

Regarding the displacements in the X-axis, a maximum displacement of 14.28 mm is observed on the left rear side of the brace, which is not localized but extends almost uniformly over the entire side of the rear face of the spinal brace (Figure 8a). On the Y-axis the maximum displacement is 26.53 mm (blue color indication), as illustrated in Figure 8b. This movement is localized in a small area on the upper right side of the rear face of the brace. Finally, on the Z-axis the maximum displacement is 16.21 mm, identified by a red colored indicator on the lower right side of the rear face of the brace (Figure 8c).

A maximum von Mises stress equal to 18.15 MPa is detected, which is locally reflected by a red colored indication at the critical areas of the spinal brace without exceeding the tensile strength of the material, which is in the order of 30–40 MPa. Stresses also develop on the front face of the brace, ranging from 1.30 MPa to 10.60 MPa.

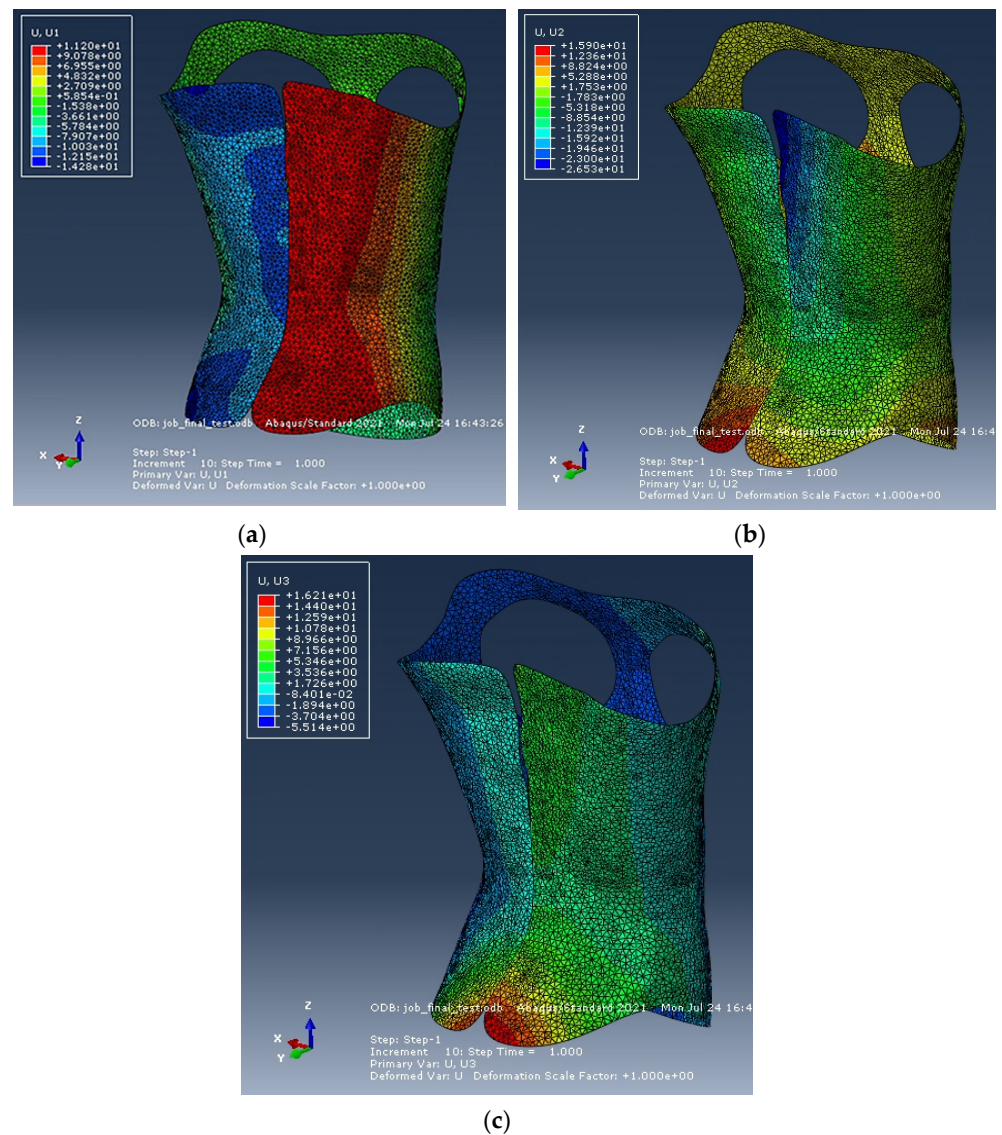


**Figure 8.** Displacements of the brace: (a) in the X-axis, (b) in the Y-axis, (c) in the Z-axis (First numerical model).

### 2.6. Parametric Analysis

Moreover, parametric analyses have been implemented, using different brace cross-sectional thicknesses and different material modulus of elasticity values. The main objective is to draw conclusions on how the above parameters affect the developing stress state of the brace as well as its overall structural performance. In Figure 9 the developing stresses of the brace for various values of the brace cross-section thickness are shown. The maximum values of observed von Mises stresses and displacements are listed in Tables 1 and 2, respectively.

**Table 1.** Max von Mises stresses for various values of the brace cross-section thickness.

Max von Mises Stress	Section Thickness
$S_{\max} = 20.29 \text{ MPa}$	$t = 5 \text{ mm}$
$S_{\max} = 18.15 \text{ MPa}$	$t = 4 \text{ mm}$
$S_{\max} = 16.60 \text{ MPa}$	$t = 3 \text{ mm}$
$S_{\max} = 14.06 \text{ MPa}$	$t = 2 \text{ mm}$

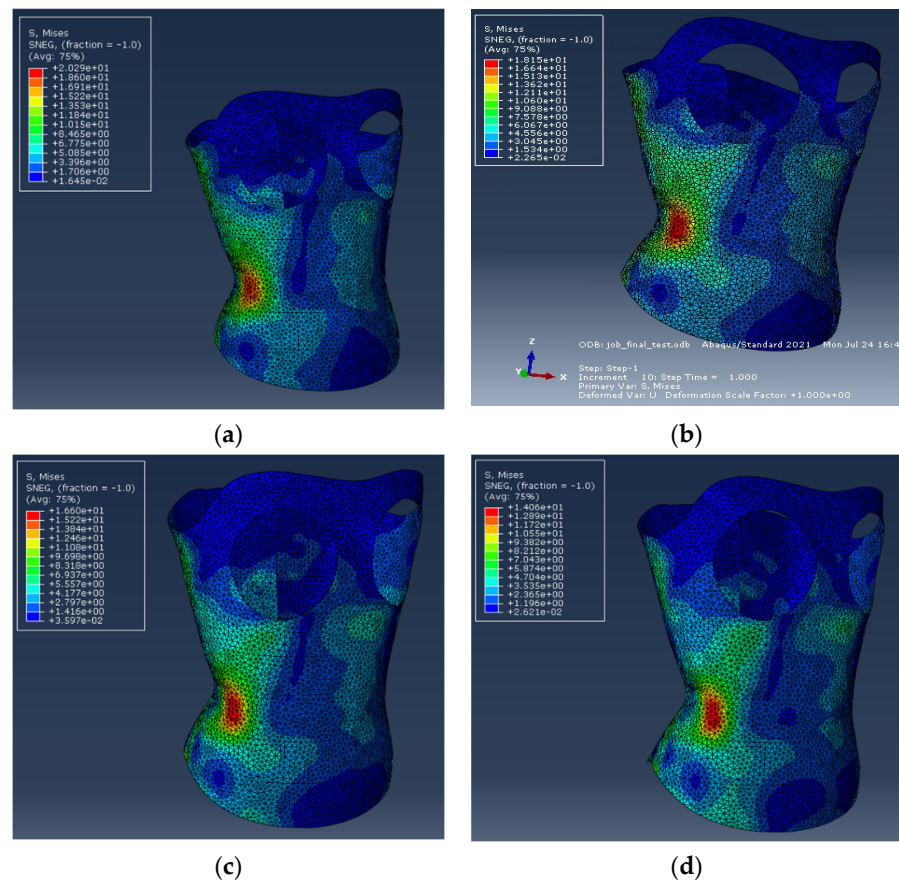


**Figure 9.** Von Mises stress results (MPa) for brace with thickness: (a)  $t = 5$  mm, (b)  $t = 4$  mm, (c)  $t = 3$  mm, (d)  $t = 2$  mm.

**Table 2.** Max displacements in the three axes for various values of the brace cross-section thickness.

Section Thickness	Displacements		
	X-Axis	Y-Axis	Z-Axis
$t = 5$ mm	13.65mm	25.81 mm	14.74 mm
$t = 4$ mm	14.28 mm	26.53 mm	16.21 mm
$t = 3$ mm	15.11 mm	27.41 mm	18.01 mm
$t = 2$ mm	16.32 mm	27.64 mm	20.35 mm

Furthermore, analyses of the brace for different values of the modulus of elasticity of the material have been conducted, with values of (a)  $E = 2340$  MPa, (b)  $E = 1520$  MPa, and (c)  $E = 320$  MPa. In Figure 10 the developing stresses of the brace for various values of the brace cross-section thickness are shown. The maximum values of observed von Mises stresses and displacements are listed in Tables 3 and 4, respectively.

**Table 3.** Max von Mises stresses for various values of modulus of elasticity of the brace material.

Max von Mises Stress	Modulus of Elasticity E
$S_{max} = 40.36$ MPa	$E = 2340$ MPa
$S_{max} = 26.91$ MPa	$E = 1520$ MPa
$S_{max} = 18.15$ MPa	$E = 1000$ MPa
$S_{max} = 6.17$ MPa	$E = 320$ MPa



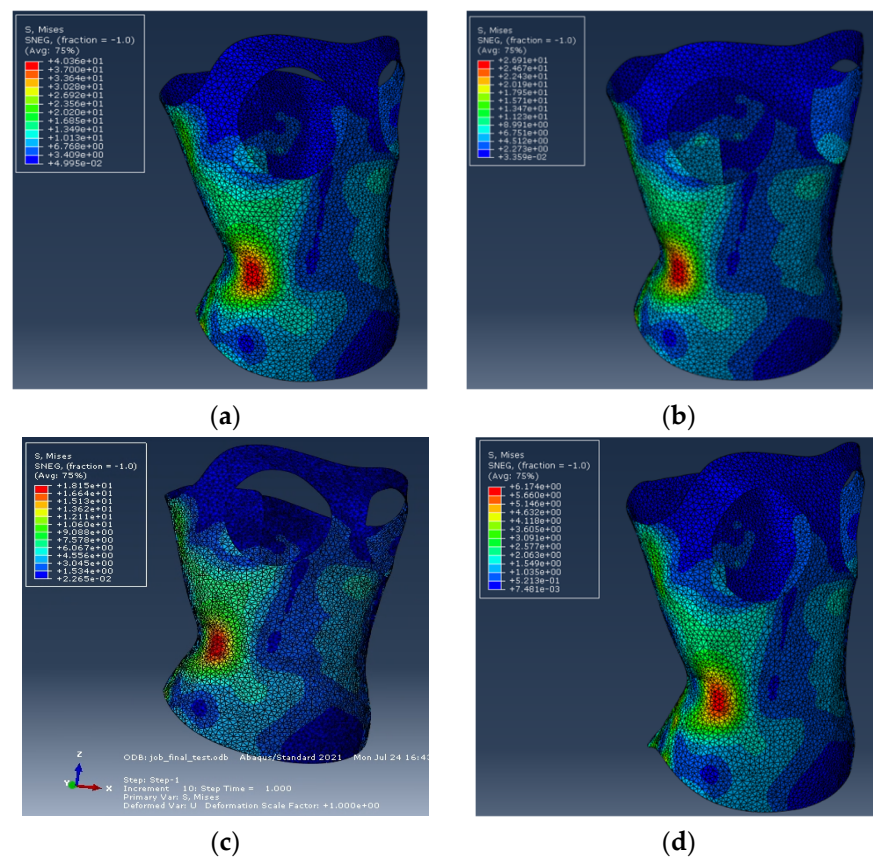


**Figure 10.** Von Mises stress results (MPa) for material with modulus of elasticity: (a)  $E = 2340$  MPa, (b)  $E = 1520$  MPa, (c)  $E = 1000$  MPa, and (d)  $E = 320$  MPa.

**Table 4.** Max displacements in the three axes for various values of the modulus of elasticity of the brace material.

Modulus of Elasticity, E	Displacements		
	X-Axis	Y-Axis	Z-Axis
$E = 2340$ Mpa	14.13 mm	25.00 mm	15.40 mm
$E = 1520$ Mpa	14.21 mm	25.83 mm	15.82 mm
$E = 1000$ Mpa	14.28 mm	26.53 mm	16.21 mm
$E = 320$ Mpa	14.44 mm	28.25 mm	17.23 mm

Interesting conclusions can be drawn regarding the effect of the thickness of the cross-section of the brace and the modulus of elasticity of its material. It is observed that as the thickness increases, a local increase in stresses is observed. As can be observed in Figure 9a, for  $t = 5$  mm the maximum stress is 20.29 MPa, for  $t = 4$  mm it is 18.15 MPa, for  $t = 3$  mm 16.60 MPa, and for  $t = 2$  mm 14.06 MPa. This can be interpreted by considering that for thicker, hence stiffer, braces, a local concentration is observed, while an overall decrease in stresses in the whole brace takes place.

According to Table 2, the maximum displacements in the X-, Y-, and Z-axes decrease as the thickness increases. For thickness  $t = 5$  mm the maximum displacement is 13.65 mm in the X-axis, 25.81 mm in the Y-axis and 14.74 mm in the Z-axis. The analysis with the smallest thickness was the one with  $t = 2$  mm, for which the maximum displacement was 16.32 mm in the X-axis, 27.64 mm in the Y-axis, and 20.35 mm in the Z-axis. Accordingly, it can be concluded that for a thickness increase of 3 mm a reduction in displacements equal to 16.36% in the X-axis, 6.62% for the Y-axis and 27.56% for the Z-axis was achieved. Therefore, the increase in thickness under the specific loading scenario conditions resulted in higher reduction in displacements in the Z-axis than in the X- and Y-axes. Furthermore,

according to the diagram shown in Figure 11, the largest displacement values are observed in the Y-axis, but the largest overall change is found in the Z-axis. Moreover, the smallest displacements are observed on the X-axis, leading to the conclusion that the brace is stiffer in the horizontal direction, specifically in the X-axis direction.

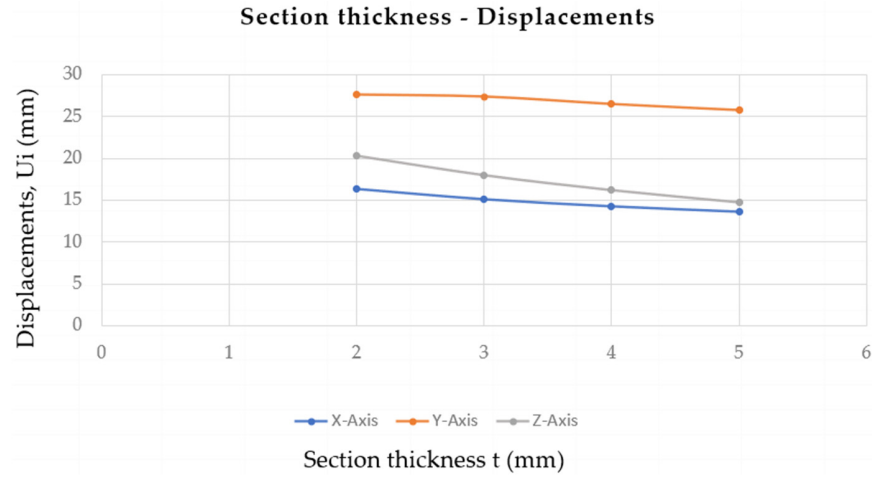


**Figure 11.** Section thickness—Displacements chart describing the change in deformation with increasing the thickness of the section of the brace.

The analysis results for different values of the elasticity modulus are illustrated in Table 3, showing that as the modulus of elasticity of the material decreases, the maximum developed stress decreases as well. The observation regarding local vs. global change in developing stresses holds here also, as in the case of increasing thickness. Namely, for  $E = 2340$  MPa the maximum stress is 40.36 MPa, for  $E = 1520$  MPa it is 26.91 MPa, for  $E = 1000$  MPa it is 18.15 MPa, and for  $E = 320$  MPa it is 6.17 MPa.

Regarding the observed displacements, they decrease in all three axes as the modulus of elasticity of the brace material increases. In particular, from Table 4 and Figure 12 it is confirmed that the smallest change in displacements is observed in the X-axis, followed by the Z-axis, while the largest change is observed in the Y-axis. In more detail, for an increase in elastic modulus of 2020 MPa, a reduction in 2.14% was achieved in the X-axis, 11.5% for the Y-axis, and 10.62% for the Z-axis. According to Table 4, the highest displacement values are observed on the Y-axis, while the displacements on the X- and Z-axes are quite close, with the X-axis plot being almost a straight line, which reveals the fairly small change in displacements on this axis.

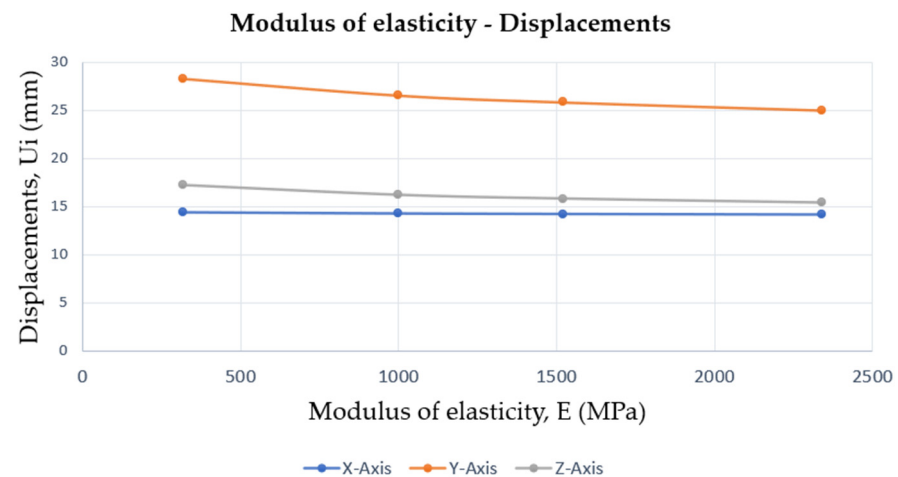


**Figure 12.** Modulus of elasticity—displacements chart describing the change in deformation with increasing modulus of elasticity.

### 3. Tension Tests of PLA Specimens

In order to evaluate the efficiency of a 3D-printed spinal brace, material characterization is necessary. The chosen 3D-printing method is FDM due to printer availability and ease of use, considering also the size of the average spinal brace. This method produces three-dimensional objects by depositing thermoplastic material layer by layer. Accordingly, 3D-printed objects are inherently anisotropic. Because the brace is aimed to be printed vertically, it is necessary to find the material properties on the horizontal and vertical axes.

#### 3.1. PLA Material

In recent studies, the most commonly used materials in FDM printed orthoses are PLA (polylactic acid) and PETG (polyethylene terephthalate glycol) [30]. PLA is a popular versatile, biodegradable, and eco-friendly thermoplastic material used in 3D printing, made of renewable resources such as corn starch and sugarcane [31]. PLA was selected for this study, considering that it has a reduced environmental impact compared to traditional plastics and functions effectively with a wide range of 3D printers. The PLA filament used is made by “Builder 3D Printers” [32] and has a diameter of 1.75 mm.

#### 3.2. Specimen Geometry and Dimensions

The tensile strength of the PLA material was measured as described by International Standards ISO 527-2 [33]. The geometry and dimensions of the “dog-bone” specimens are shown in Figure 13.

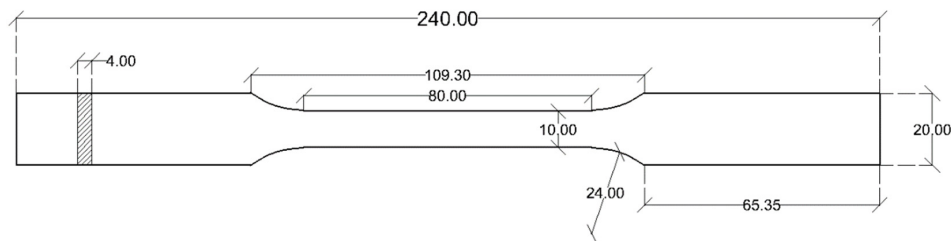


**Figure 13.** Geometry and dimensions of tensile strength specimen in mm.

#### 3.3. Specimen Printing

Ten specimens were printed, five vertically ( $90^\circ$ ) and five horizontally ( $0^\circ$ ) (Figure 14a), comprising 100% infill and three outer layers each (Figure 14b), using a nozzle diameter of 0.40 mm and a layer height of 0.30 mm. The software used to “slice” the 3D model is “Simplify 3D” [34] and the 3D printer used is “Builder Extreme 1000 PRO” [35].

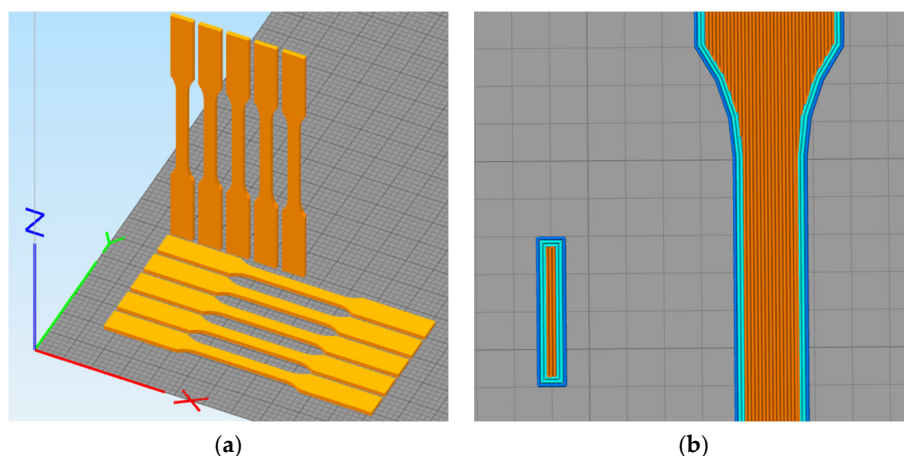


**Figure 14.** (a) Specimen orientation and (b) inner geometry of 3D-printed specimens. The light and dark blue color presents the outer walls and the orange color the infill.

### 3.4. Tensile Tests

Tensile tests were performed in a displacement-controlled manner using a universal testing machine of type INSTRON 300LX. Before the tensile strength testing, all specimens were weighed [36] and measured using a micrometer [37] in various locations. The testing speed was set at 1 mm/min according to ISO 527-2. In Figure 15a,b a specimen is seen placed in the tensile tester [38] at the start and end of the experiment.

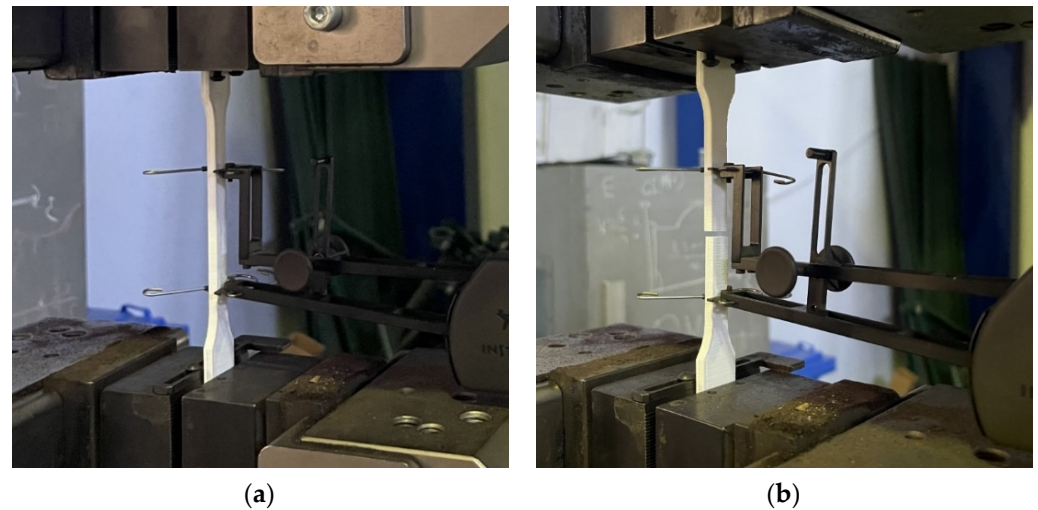


**Figure 15.** (a) Specimen placed in the testing machine and (b) specimen placed in the testing machine after the end of the experiment.

### 3.5. Tensile Test Results

True stress–true strain curves were plotted based on the tensile testing results of the specimens. Imposed longitudinal displacements [mm] and required loads [N] are measured by the testing machine. This data was then processed to produce true stress–true strain values. Figures 16 and 17 show the obtained stress–strain curves for PLA printed at 0° and 90°.

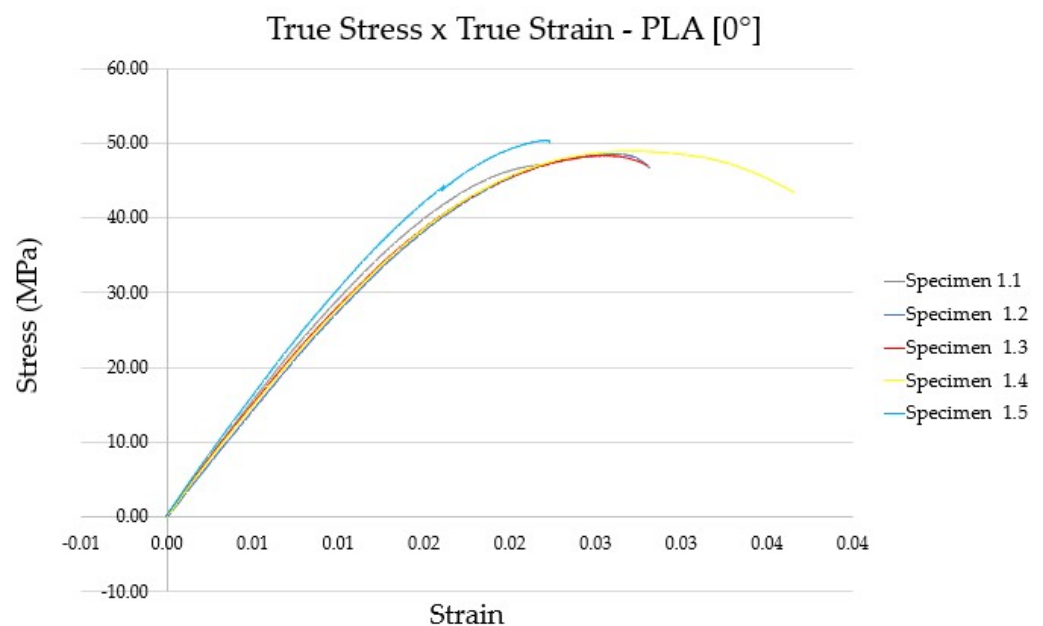


**Figure 16.** True stress–true strain curves for test specimens of direction 1 [0°].

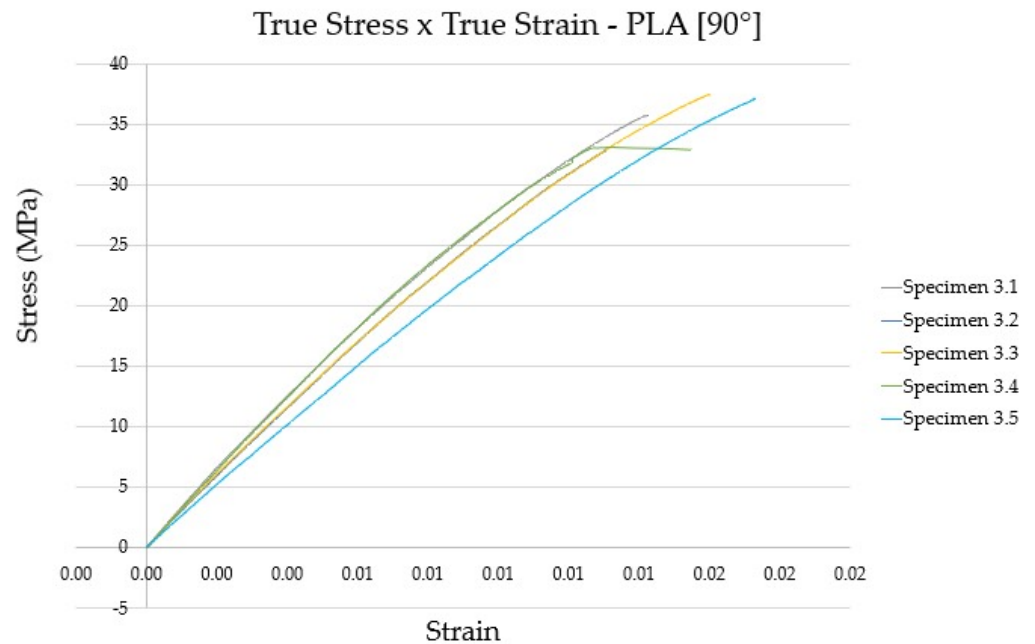


Figure 17. True stress–true strain curves for test specimens of direction 2 [90°].

The modulus of elasticity was calculated from the stress–strain diagrams by linear fitting in the part of the purely elastic region for every specimen. Overall, the statistical interpretation of the experimental test results was based on ISO 2602 [39]. The aggregated results of tensile tests are presented in Table 5.

Table 5. Summary of tensile test results.

Specimen	Modulus of Elasticity [MPa]	Ultimate Tensile Stress [MPa]	Ultimate Strain
1.1	3127.1	47.06	0.0351
1.2	2857.4	48.49	0.0394
1.3	3004.0	48.36	0.0469
1.4	2988.4	48.97	0.0505
1.5	3241.4	50.42	0.0223
3.1	3121.2	35.76	0.0217
3.2	2871.3	32.82	0.0131
3.3	2887.7	37.46	0.0200
3.4	3089.4	33.10	0.0297
3.5	2518.7	34.17	0.0152

The mean value of the tensile strength of PLA was found to be 48.66 MPa in direction 0° and 34.66 MPa in direction 90°, close to the results reported by other researchers [10], and significantly higher than the strength of traditional thermoplastic materials as found in publications [17,24]. Moreover, the mean value of the modulus of elasticity was calculated to be equal to 3043.66 MPa for direction 0° and 2897.66 MPa for direction 90°, which are close to values obtained in similar experiments [8,15,39] for PLA material.

#### 4. Numerical Simulations of a 3D-Printed Brace

In order to evaluate the efficiency of 3D-printed braces made of PLA material, the numerical simulations were repeated, adopting modulus of elasticity values from Table 6 and Poisson's ratio [ $\nu$ ] and shear modulus [ $G$ ] values from the literature [40], as presented in Table 7.



Table 6. Descriptive statistics of 3D-printed PLA specimens.

Orientation	Measure	Range	Min	Max	Mean	St. Dev	Confidence Interval (Two Sided)			
							95%		99%	
							$X_{mean}>$	$X_{mean}<$	$X_{mean}>$	$X_{mean}<$
0°	E [MPa]	384.00	2857.40	3241.40	3043.66	146.10	2848.97	3238.35	2719.95	3367.37
	$\sigma_{ult}$ [MPa]	3.35	47.06	50.42	48.66	1.21	46.96	50.36	45.83	51.49
90°	E [MPa]	602.50	2518.70	3121.20	2897.66	240.38	2592.19	3203.13	2389.75	3405.57
	$\sigma_{ult}$ [MPa]	4.63	32.82	37.46	34.66	1.94	32.31	37.01	30.76	38.57

The obtained results are shown in Figures 18–20.

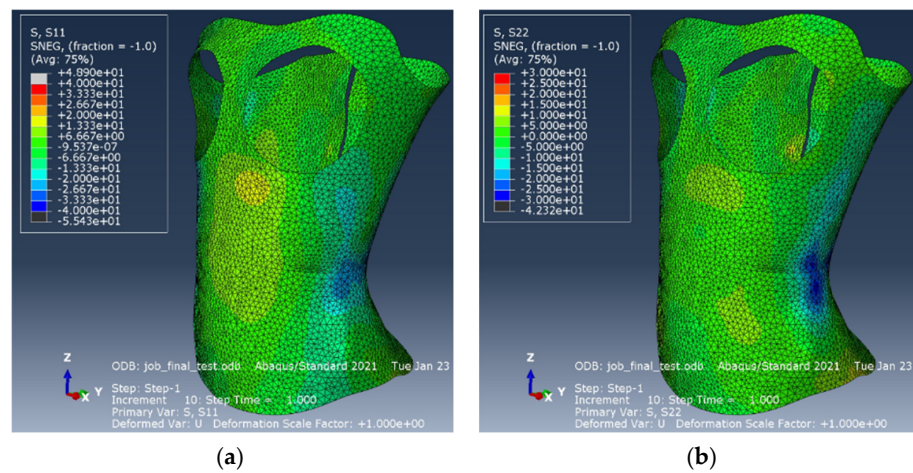


Figure 18. Results of primary stresses on the spinal brace: (a) S11; (b) S22.

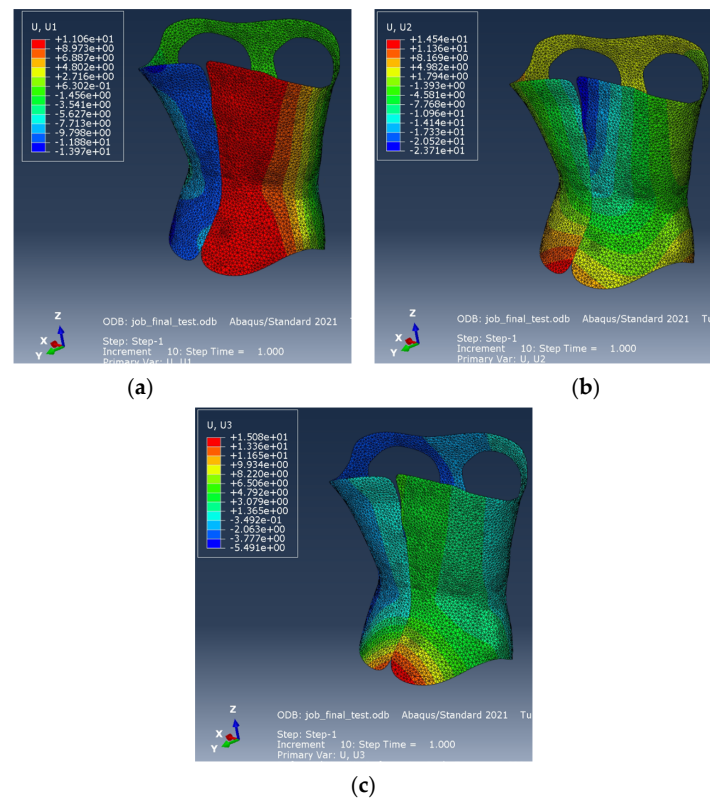
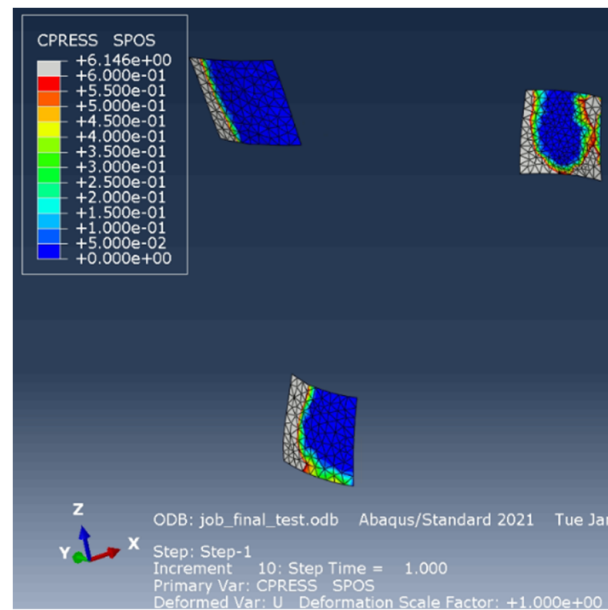


Figure 19. Displacements of the brace: (a) in the X-axis, (b) in the Y-axis, (c) in the Z-axis (Second numerical model).



**Figure 20.** Contact pressures on the surfaces representing the human body (Second Numerical model).

**Table 7.** Material properties of 3D-printed PLA simulation.

Material	E1	E2	$\nu_{12}$	G12	G13	G23
	MPa	MPa	-	MPa	MPa	MPa
PLA	3043.66	2898	0.330	1140	1140	1140

In primary stress S11 results (Figure 18a) a local stress concentration of 48.9 MPa is observed, slightly exceeding the tensile strength of the material in this direction, which was calculated equal to 48.66 MPa. However, almost the whole surface of the brace is stressed with values below 30 MPa, well below the tensile strength of the material. Similarly, in the S22 primary stress results (Figure 18b), stresses below 25 MPa are observed over the entire surface of the brace, which is smaller than the tensile strength in direction 2 which was found to be equal to 34.66 MPa. Comparing the contact pressure results of Figure 20 with those of Figure 7, it is observed that in the simulation with PLA material, higher pressures are developed due to the higher modulus of elasticity and resulting higher stiffness of the brace.

## 5. Outline of Next Steps

In the subsequent phases of our study, we are pursuing the following objectives: Expanding the numerical model to encompass the interaction between the human body and the spinal brace during typical movements. Ensuring close collaboration between medical and engineering teams is pivotal to the success of this initiative. To optimize the spinal brace's effectiveness, we will employ topology optimization, strategically removing material to minimize energy resulting from applied loads. Utilizing design variables as densities will pinpoint lighter sections, reducing overall weight without compromising performance. Both the original and optimized spinal braces will be seamlessly 3D printed, eliminating the need for post-print assembly. Investigating 4D printing for brace optimization will explore the utilization of responsive materials adapting to stimuli from human body motions [41]. The optimized brace will undergo experimental tests using a deformable replica of the human body, with special sensors and strain gauges measuring stress and strain during strap tightening to validate numerical results. The clinical study's objective is to validate research findings under realistic conditions. Further research will be necessary to address issues such as the reliability, fatigue and material degradation of the polymers used to print these braces in relation to various printing techniques and

seasonal fluctuations of the environmental moisture and temperature [42]. The tribological interactions between 3D-printed materials and skin is another important factor [43], which could lead to dermatological discomfort or nonacceptable skin irritation, adding another important parameter to the study.

## 6. Discussion

Our research, compared to other studies [10,15–17], places significant emphasis on understanding the contact mechanics between spinal braces and the human body. The accurate simulation of the interaction between them is crucial in creating a realistic numerical model. This interaction, involving the development of corrective forces, pressures, and friction during patient movement, when combined with established interaction laws, such as the pressure–overclosure relation, enables precise simulation of real-world contact dynamics which further improves the reliability and accuracy of the numerical model. This can lead to a more accurate optimized brace design.

The parametric analysis of the spinal brace numerical model revealed that increasing either the cross-sectional thickness or elastic modulus of the brace material leads to elevated maximum von Mises stresses and reduced displacements. Additionally, the tensile testing demonstrated that the 3D-printed material has a higher modulus of elasticity compared to traditional brace materials, which leads to a stiffer 3D-printed spinal brace when compared to a traditional one, as seen in other studies [8,9].

An important limitation is the lack of real-life application of the spinal brace with regards to pragmatic contact points between the brace and the human body. Furthermore, our model is inevitably based on a static computerized torso, contrary to the dynamic status of the ribcage during standstill and movements, thus we still cannot know the true wearability of our described product.

## 7. Summary and Conclusions

A finite element model of a spinal brace and its interaction with the human body was developed, adopting the geometry from a 3D scan of an already manufactured brace. The simulation focused on modeling the functioning of tethering straps and supporting pads to emulate a loading scenario. The simulation considered the nonlinear interaction between the body and the brace, factoring in elements such as skin deformation and friction in both normal and tangential directions. Numerical results were obtained for traditional brace materials as well as for 3D-printed PLA material obtained from tensile tests. It was concluded that 3D-printed braces may be designed to feature suitable stiffness and strength while being easily adjusted to each specific patient.

**Author Contributions:** Conceptualization, N.D.L., C.J.G. and K.S.; methodology, C.J.G. and N.D.L.; finite element analyses and parametric studies, I.R.; conversion of scanning file, G.K. and S.V.; orthopedic expertise, K.S. and D.G.; finite element expertise, C.J.G. and N.D.L.; optimization expertise, N.D.L. and G.K.; writing—original draft preparation, I.R. and G.K.; writing—review and editing, C.J.G. and N.D.L.; visualization, F.P., G.K., S.V. and I.R.; supervision, C.J.G. and N.D.L.; and project administration, N.D.L. All authors have read and agreed to the published version of the manuscript.

**Funding:** This research was supported by the OrThOP3Dics project: “Topology optimization of 3D printed patient-specific spinal braces” (No.: TAEDK-06191) belonging to the National Recovery and Resilience Plan, Greece 2.0 Project.

**Institutional Review Board Statement:** Not applicable.

**Informed Consent Statement:** Not applicable.

**Data Availability Statement:** The data used in the study is available with the authors and can be shared upon reasonable request.

**Conflicts of Interest:** The authors declare no conflicts of interest.

## Abbreviations

The following abbreviations are used in this manuscript:

3D	Three dimensional
4D	Four dimensional
CAD	Computer aided design
CAE	Computer aided engineering
FE	Finite element
FEA	Finite element analysis
FDM	Fused deposition modeling
PLA	Polylactic acid
PETG	Polyethylene terephthalate glycol

## References

- Marketos, S.G.; Skiadas, P. Hippocrates: The Father of Spine Surgery. *Spine* **1999**, *24*, 1381. [CrossRef]
- Yağci, G.; Bek, N. A Historical Perspective of the Management of Scoliosis. *Erciyes Med. J.* **2022**, *44*, 439–446.
- Zarea, M.; Aminian, G.; Khosravi, M.; Baghaei, R. Effect of Milwaukee Brace on Quality of Life in Adolescents with Idiopathic Scoliosis. *J. Clin. Physiother. Res.* **2020**, *5*, e13.
- Olafsson, Y.; Saraste, H.; Söderlund, V.; Hoffsten, M. Boston Brace in the Treatment of Idiopathic Scoliosis. *J. Pediatr. Orthop.* **1995**, *15*, 524. [CrossRef] [PubMed]
- Khan, M.J.; Srinivasan, V.M.; Jea, A.H. The History of Bracing for Scoliosis. *Clin. Pediatr.* **2015**, *55*, 320–325. [CrossRef]
- Kim, J.; Heo, G.; Lagravère, M.O. Accuracy of Laser-Scanned Models Compared to Plaster Models and Cone-Beam Computed Tomography. *Angle Orthod.* **2013**, *84*, 443–450. [CrossRef]
- Taneva, E.; Kusnoto, B.; Evans, C.A. *3D Scanning, Imaging, and Printing in Orthodontics*; IntechOpen: London, UK, 2015; Available online: <https://www.intechopen.com/chapters/48165> (accessed on 24 January 2024).
- Wu, Y.; Liu, J.; Kang, L.; Tian, J.; Zhang, X.; Hu, J.; Huang, Y.; Liu, F.; Wang, H.; Wu, Z. An Overview of 3D Printed Metal Implants in Orthopedic Applications: Present and Future Perspectives. *Heliyon* **2023**, *9*, e17718. [CrossRef]
- Choo, Y.J.; Boudier-Revéret, M.; Chang, M.C. 3D Printing Technology Applied to Orthosis Manufacturing: Narrative Review. *Ann. Palliat. Med.* **2020**, *9*, 4262–4270. [CrossRef] [PubMed]
- Ronca, A.; Abbate, V.; Redaelli, D.F.; Storm, F.; Cesaro, G.; De, C.; Sorrentino, A.; Colombo, G.; Paolo, F.; Ambrosio, L. A Comparative Study for Material Selection in 3D Printing of Scoliosis Back Brace. *Materials* **2022**, *15*, 5724. [CrossRef]
- Storm, F.A.; Redaelli, D.F.; Biffi, E.; Reni, G.; Frascini, P. Additive Manufacturing of Spinal Braces: Evaluation of Production Process and Postural Stability in Patients with Scoliosis. *Materials* **2022**, *15*, 6221. [CrossRef]
- Zolfagharian, A.; Gregory, T.M.; Bodaghi, M.; Gharaie, S.; Fay, P. Patient-Specific 3D-Printed Splint for Mallet Finger Injury. *Int. J. Bioprinting* **2020**, *6*, 259. [CrossRef] [PubMed]
- Zhang, Y.; Kwok, T.-H. Customization and Topology Optimization of Compression Casts/Braces on Two-Manifold Surfaces. *Comput. Aided Des.* **2019**, *111*, 113–122. [CrossRef]
- Redaelli, D.F.; Abbate, V.; Storm, F.A.; Ronca, A.; Sorrentino, A.; De Capitani, C.; Biffi, E.; Ambrosio, L.; Colombo, G.; Frascini, P. 3D printing orthopedic scoliosis braces: A test comparing FDM with thermoforming. *Int. J. Adv. Manuf. Technol.* **2020**, *111*, 1707–1720. [CrossRef]
- Zolfagharian, A.; Khosravani, M.R.; Kaynak, A. Fracture Resistance Analysis of 3D-Printed Polymers. *Polymers* **2020**, *12*, 302. [CrossRef] [PubMed]
- Mafi, M.; Niyaval, A.M.K.; Khanmohammadi, S. Brace Simulation for Patients with Scoliosis: Biomechanical Comparison with Three Different Polymeric Materials. *BKK Med. J.* **2019**, *15*, 161. [CrossRef]
- Grycuk, S.; Mrozak, P. Scoliosis Brace Finite Element Model and Preliminary Experimental Testing Using Electronic Speckle Pattern Interferometry. *Appl. Sci.* **2022**, *12*, 3876. [CrossRef]
- Liao, Y.-C.; Feng, C.-K.; Tsai, M.-W.; Chen, C.-S.; Cheng, C.-K.; Ou, Y.-C. Shape Modification of the Boston Brace Using a Finite-Element Method with Topology Optimization. *Spine* **2007**, *32*, 3014–3019. [CrossRef]
- Périé, D.; Aubin, C.E.; Lacroix, M.; Lafon, Y.; Labelle, H. Biomechanical Modelling of Orthotic Treatment of the Scoliotic Spine Including a Detailed Representation of the Brace-Torso Interface. *Med. Biol. Eng. Comput.* **2004**, *42*, 339–344. [CrossRef]
- Athar, A.; Fontanari, V.; Schmölz, W.; Lafon, Y.; Agrawal, S.-K. Active Soft Brace for Scoliotic Spine: A Finite Element Study to Evaluate in-Brace Correction. *Robotics* **2022**, *11*, 37.
- Simulia Abaqus CAE. Available online: <https://www.3ds.com/products/simulia/abaqus/cae> (accessed on 24 January 2024).
- Meshmixer by Autodesk. Available online: <https://meshmixer.com> (accessed on 24 January 2024).
- Yun, J.-H.; Jeon, Y.-J.; Kang, M.-S. Numerical Investigation of the Elastic Properties of Polypropylene/Ultra High Molecular Weight Polyethylene Fiber inside a Composite Material Based on Its Aspect Ratio and Volume Fraction. *Polymers* **2022**, *14*, 4851. [CrossRef]
- Hoque, B.-M.; Solaiman; Alam, H.-A.-B.-M.; Mahmud, H.; Nobi, A. Mechanical, Degradation and Water Uptake Properties of Fabric Reinforced Polypropylene Based Composites: Effect of Alkali on Composites. *Fibers* **2018**, *6*, 94. [CrossRef]

25. Graham, H.-K.; McConnell, J.-C.; Limbert, G.; Sherratt, J. How stiff is skin? *Exp. Dermatol.* **2019**, *28* (Suppl. S1), 4–9. [[CrossRef](#)]
26. Cua, A.-B.; Wilhelm, K.-P.; Maibach, H.-I. Elastic properties of human skin: Relation to age, sex, and anatomical region. *Arch. Dermatol. Res.* **1990**, *282*, 283–288. [[CrossRef](#)]
27. Babaei, T.; Kamyab, M.; Ahmadi, A.; Sanjari, M.-A.; Ganjavian, M.-S. Measurement of Milwaukee Brace Pad Pressure in Adolescent Round Back Deformity Treatment. *Asian Spine J. Clin. Study* **2017**, *11*, 627–633. [[CrossRef](#)]
28. Aubin, C.; Cobetto, N.; Clin, J.; Desbiens-Blais, F.; Labelle, H.; Le May, S.; Parent, S. Improved Brace Design Combining CAD/CAM And Finite Element Simulation For The Conservative Treatment Of Adolescent Idiopathic Scoliosis (AIS): Preliminary Results Of A Randomized Control Trial. In Proceedings of the 10th Meeting of the International Research Society of Spinal Deformities (IRSSD 2014 Sapporo), Sapporo, Japan, 29 June–2 July 2014.
29. Pham, V.-M.; Houilliez, A.; Schill, A.; Carpentier, A.; Herbaux, B.; Thevenon, A. Study of The Pressures Applied by A Cheneau Brace for Correction of Adolescent Idiopathic Scoliosis. *Prosthet. Orthot. Int.* **2008**, *32*, 345–355. [[CrossRef](#)]
30. Murariu, M.; Dubois, P. PLA Composites: From Production to Properties. *Adv. Drug Deliv. Rev.* **2016**, *107*, 17–46. [[CrossRef](#)]
31. PLA by Builder 3D Printers. Available online: <https://builder3dprinters.com/product/filament-pla-4-5kg/> (accessed on 24 January 2024).
32. ISO 527-2:2012; Plastics. Determination of Tensile Properties. Part 2: Test Conditions for Moulding and Extrusion Plastics. ISO: Geneva, Switzerland, 2012.
33. Simplify3D Software. Available online: <https://www.simplify3d.com> (accessed on 24 January 2024).
34. Builder Extreme 1000 PRO. Available online: <https://builder3dprinters.com/product/builder-extreme-1000/> (accessed on 24 January 2024).
35. Adam Equipment PGW 3502i. Available online: <https://www.affordablescales.com/adam-equipment/pgw/pgw-3502i.asp> (accessed on 24 January 2024).
36. Mitutoyo Series 103 Micrometer. Available online: [https://shop.mitutoyo.eu/web/mitutoyo/en/mitutoyo/01.02.01.031/Series%20103/PG/103\\_WA/index.xhtml](https://shop.mitutoyo.eu/web/mitutoyo/en/mitutoyo/01.02.01.031/Series%20103/PG/103_WA/index.xhtml) (accessed on 24 January 2024).
37. INSTRON Tensile Testers. Available online: <https://www.instron.com/en/resources/test-types/tensile-test> (accessed on 24 January 2024).
38. ISO 2602:1980; Statistical Interpretation of Test Results. Estimation of the Mean. Confidence Interval. ISO: Geneva, Switzerland, 1980.
39. Agaliotis, E.-M.; Ake-Concha, B.-D.; May-Pat, A.; Morales-Arias, J.-P.; Bernal, C.; Valadez-Gonzalez, A.; Herrera-Franco, P.-J.; Proust, G.; Koh-Dzul, J.-F.; Carrillo, J.-G.; et al. Tensile Behavior of 3D Printed Polylactic Acid (PLA) Based Composites Reinforced with Natural Fiber. *Polymers* **2022**, *14*, 3976. [[CrossRef](#)]
40. Ferreira, R.-T.-L.; Amatte, I.-C.; Dutra, T.-A.; Bürger, D. Experimental characterization and micrography of 3D printed PLA and PLA reinforced with short carbon fibers. *Compos. Part B Eng.* **2017**, *124*, 88–100. [[CrossRef](#)]
41. Zolfagharian, A.; Denk, M.; Bodaghi, M.; Kouzani, A.Z.; Kaynak, A. Topology-Optimized 4D Printing of a Soft Actuator. *Acta Mech. Solida Sin.* **2019**, *33*, 418–430. [[CrossRef](#)]
42. Banjo, A.D.; Agrawal, V.; Auad, M.L.; Celestine, A.-D.N. Moisture-Induced Changes in the Mechanical Behavior of 3D Printed Polymers. *Compos. Part C Open Access* **2022**, *7*, 100243. [[CrossRef](#)]
43. Kasar, A.K.; Chan, A.; Shamanaev, V.; Menezes, P.L. Tribological Interactions of 3D Printed Polyurethane and Polyamide with Water-Responsive Skin Model. *Friction* **2021**, *10*, 159–166. [[CrossRef](#)]

**Disclaimer/Publisher’s Note:** The statements, opinions and data contained in all publications are solely those of the individual author(s) and contributor(s) and not of MDPI and/or the editor(s). MDPI and/or the editor(s) disclaim responsibility for any injury to people or property resulting from any ideas, methods, instructions or products referred to in the content.